Comparative performance evaluation of microarchitected lattices processed via SLS, MJ, and DLP 3D printing methods: Experimental investigation and modelling

Johannes Schneider[1], S. Kumar[1,2*]

[1]Materials & Manufacturing Research Group, James Watt School of Engineering, University of Glasgow, Glasgow G12 8QQ, UK.

[2]Glasgow Computational Engineering Centre, University of Glasgow, Glasgow G12 8LT, UK.

S1 Stretching and bending dominated cellular materials

The stress-strain response of cellular structures under compression exhibits three typical regimes: a linear elastic regime, followed by a plateau regime and finally a densification regime, where the stress increases steeply as a function of strain. The Young's modulus describes the stiffness of the cellular material in the elastic regime and is mostly driven by the bending- and/or stretching-dominated nature of the cellular structure [1].

At similar densities, stretch-dominated cellular materials outperform bend-dominated ones, such us foams, in terms of stiffness and strength [1,2]. The usual coupling between Young's modulus, E and the relative density, $\bar{\rho}$, and yield strength, σ and $\bar{\rho}$ are given by

$$\frac{\mathrm{E}}{\mathrm{E_s}} = C_1 \left(\frac{\rho}{\rho_s}\right)^{\mathrm{n}} \tag{1}$$

and

$$\frac{\sigma}{\sigma_s} = C_2 \left(\frac{\rho}{\rho_s}\right)^{\mathrm{m}} \tag{2}$$

where, the coefficients C_i and the exponents n and m are scaling parameters and are governed by the unit cell topology. The parameters with subscript s refer to the bulk material. The exponents n and m define the dominant deformation behaviour of the cellular structure. While for stretch-dominated materials, the relationship is ideally linear with $n = 1$, for bend-dominated structures the exponent is highly non-linear with $n \approx 2$.

The plateau region of the stress-strain curve is governed by the inelastic processes such as plastic deformation and/or damage of the material and is characterised by the chosen unit cell topology, material, and the relative density. Particularly brittle materials show a non-flat plateau region with multiple drops in the stress-strain response characterised by the failure of the ligaments in the lattice material. In the third stage, opposing walls or struts come into contact and form crush bands, resulting in work hardening and densification of the cellular structure.

S2 Elastic plastic material model

This paragraph offers supplementary details regarding the elastic-plastic material employed in the study.

The elastic-plastic material model is described within the Abaqus theory manual [3] and assumes that the deformation can be divided into an elastic and inelastic (plastic) part, $\boldsymbol{F} = \boldsymbol{F}^{el} \cdot \boldsymbol{F}^{pl}$, where the total deformation gradient, $\boldsymbol{F}$, is composed of the fully recoverable part $\boldsymbol{F}^{el}$, and the plastic part $\boldsymbol{F}^{pl}$, defined by $\boldsymbol{F}^{pl} = [\boldsymbol{F}^{el}]^{-1} \cdot \boldsymbol{F}$. The strain rate is defined as the decomposition of $\dot{\boldsymbol{\varepsilon}} = \dot{\boldsymbol{\varepsilon}}^{el} + \dot{\boldsymbol{\varepsilon}}^{pl}$, assuming that the elastic response is small in models in which it is used. The elastic stress is defined by $\boldsymbol{\sigma} = \delta U / \delta \varepsilon^{el}$, with the strain energy density potential U. The limit of purely elastic response is defined by the yield function, f, given by $f(\boldsymbol{\sigma}, \theta, H_\alpha) < 0$, where θ is the temperature and H_α are hardening parameters. The inelastic part is defined by the flow rule, given by $d\varepsilon^{pl} = \sum_i d\lambda_i \, \delta g_i / \delta \boldsymbol{\sigma}$, with $g_i\left(\boldsymbol{\sigma}, \theta, H_{i,\alpha}\right)$ being the flow potential for the *i*th system, and $d\lambda_i$ being a scalar measuring the amount of plastic flow rate on the *i*th system. Finally, the plasticity model is defined by the set of evolution equations for the hardening parameters, written as $dH_{i,\alpha} = d\lambda_i h_{i,\alpha}\left(\boldsymbol{\sigma}, \theta, H_{i,\beta}\right)$. Here, $h_{i,\alpha}$ is the hardening law for $H_{i,\alpha}$.

S3 Tables

Table S1 and Table S2 present the geometric parameters and relative densities of the structures processed via SLS and PolyJet AM techniques, respectively.

Table S1. Geometric parameters and relative density of lattice structures, processed via SLS using PA12

PA12		**Octet**		**Kelvin**		**Gyroid**		**SC**	
Conf.	L [mm]	$\bar{\rho}$	d [µm]	$\bar{\rho}$	d [µm]	$\bar{\rho}$	t [µm]	$\bar{\rho}$	t [µm]
4×4×3	7	0.23	1038	0.23	1494	0.23	526	0.23	607

Table S2. Geometric parameters and relative densities of lattice structures, processed by PolyJet AM using VeroWhite

VeroWhite		**Octet**		**Kelvin**		**Gyroid**		**SC**	
Conf.	L [mm]	$\bar{\rho}$	d [µm]	$\bar{\rho}$	d [µm]	$\bar{\rho}$	t [µm]	$\bar{\rho}$	t [µm]
4×4×3	7	0.23	1038	0.23	1494	0.23	526	0.23	607
2×2×2	10	-	-	-	-	0.12	394	-	-
3×3×3	6.67	-	-	-	-	0.18	394	-	-
4×4×4	5	-	-	-	-	0.24	394	-	-
5×5×5	4	-	-	-	-	0.3	394	-	-
6×6×6	3.33	-	-	-	-	0.36	394	-	-

Table S3. Summary of mechanical properties measured for a variety of lattice structures printed using VeroWhite via PolyJet AM technique.

Configuration	$\bar{\rho}$	**E [MPa]**	**σ [MPa]**	**W [kJ/m^3]**	**η**
2×2×2	0.06	11.10	0.32	161.67	0.45
3×3×3	0.13	32.98	1.02	609.37	0.45
4×4×4	0.21	38.57	2.00	954.99	0.47
5×5×5	0.3	66.04	2.95	1347.13	0.43
6×6×6	0.36	51.25	3.11	1359.50	0.41

Table S4. Concrete damage plasticity parameters for VeroWhite

Dilation Angle	**Eccentricity**	**fb0/fc0**	**K**
40	0.1	1	1

S4 Figures

Figure S1 illustrates the standard configuration of a lattice structure with applied boundary conditions for finite element analysis. Meanwhile, Figure S2 showcases Eigenmode 1 obtained from buckling analysis for the Gyroid lattice at various relative densities.

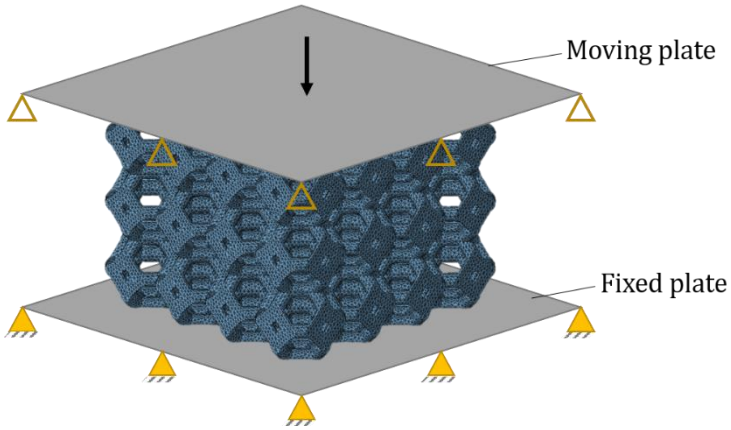

Fig. S1. Typical FE model of a lattice structure with appropriate boundary and loading conditions.

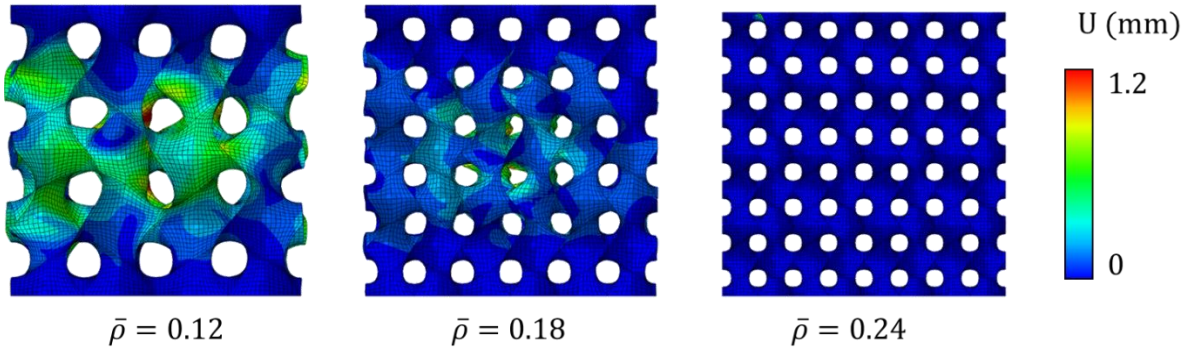

Fig. S2. Buckling analysis: Eigenmode 1 for Gyroid structure for different relative densities

Fig. S3. Universal testing machines used in this study: Instron 5969 equipped with 50 kN load cell (left) Zwick//Roell Z005 equipped with 2.5 kN load cell (right)

References

[1] V.S. Deshpande, M. Ashby, N. Fleck, Foam topology: Bending versus stretching dominated architectures, Acta Mater. 49 (2001) 1035–1040. https://doi.org/10.1016/S1359-6454(00)00379-7.

[2] M. Ashby, The Properties of Foams and Lattices, Philos. Trans. A. Math. Phys. Eng. Sci. 364 (2006) 15–30. https://doi.org/10.1098/rsta.2005.1678.

[3] Dassault Systemes, Abaqus: About plasticity models, (2020). help.3ds.com.